Journal of Pharmaceutical Analysis 15 (2025) 101048

Contents lists available at ScienceDirect

Journal of Pharmaceutical Analysis

journal homepage: www.elsevier.com/locate/jpa

Original article

Isovalerylspiramycin I alleviates liver injury and liver fibrosis by targeting the nucleotide-binding protein 2 (NUBP2)-vascular non-inflammatory molecule-1 (VNN1) pathway

Na Zhang [a, 1], Weixiao Niu [c, 1], Weiping Niu [a], Yiming Li [a], Simin Guo [a], Yang Li [a], Weiqing He [b, *], Hongwei He [a, **]

[a] NHC Key Laboratory of Biotechnology for Microbial Drugs, Institute of Medicinal Biotechnology, Chinese Academy of Medical Sciences and Peking Union Medical College, Beijing, 100050, China
[b] CAMS Key Laboratory of Synthetic Biology for Drug Innovation, Institute of Medicinal Biotechnology, Chinese Academy of Medical Sciences and Peking Union Medical College, Beijing, 100050, China
[c] Medical Department of Shandong Provincial Hospital Affiliated to Shandong First Medical University, Jinan, 250021, China

ARTICLE INFO

Article history:
Received 10 April 2024
Received in revised form
25 June 2024
Accepted 16 July 2024
Available online 18 July 2024

Keywords:
Liver fibrosis
Isovalerylspiramycin I
Carrimycin
Nucleotide-binding protein 2
Vascular non-inflammatory molecule-1

ABSTRACT

Liver fibrosis is a vital cause of morbidity in patients with liver diseases and developing novel anti-fibrotic drugs is imperative. Isovalerylspiramycin I (ISP I) as a major component of carrimycin applied to upper respiratory infections, was first found to possess anti-fibrotic potential. The present study aims to evaluate the functions and mechanisms of ISP I in protecting against liver fibrosis. According to our results, ISP I not only reduced the expressions of fibrogenic markers in LX-2 cells but also appeared great protective effects on liver injury and liver fibrosis in bile duct ligation (BDL) rats and carbon tetrachloride (CCl_4) mice. We proved that nucleotide-binding protein 2 (NUBP2) was the direct target of ISP I. ISP I through targeting NUBP2, increased the amount of vascular non-inflammatory molecule-1 (VNN1) on the cell membrane, which will inhibit oxidative stress and fibrosis. Simultaneously, the original carrimycin's protective effect on liver damage and fibrosis was verified. Therefore, our study provides potential agents for patients with liver fibrosis-related diseases, and the clear mechanism supports wide application in the clinic.

1. Introduction

Fibrosis is a tissue repair compensatory response majorly characterized by excess accumulation of fibrous connective tissue resulting in progressive architectural remodeling [1]. Liver fibrosis is an important stage in chronic liver disease development closely related to the progression of cirrhosis and even cancer. However, there are still rarely approved anti-liver fibrosis drugs for clinical use. Effective therapy for rapid and advanced fibrosis progression is still imperative, especially since the reversal of liver fibrosis is a challenge nowadays.

Activation of hepatic stellate cells (HSCs) is well established as a central driver of fibrosis in liver injury, which refers to HSCs' *trans*-differentiation into myofibroblasts from vitamin A storage cells [2]. The HSCs proliferation and activation were always induced by multiple chemokines, such as transforming growth factor-β (TGF-β), and interleukin-1 beta (IL-1β) [2,3]. Activated HSCs produce matrix proteins, including fibrillar collagen type I alpha 1 (COL1A1), the contractile protein alpha-smooth muscle actin (α-SMA, encoded by Actin Alpha 2), and the tissue inhibitors of metalloproteinase (TIMPs). Besides, oxidative stress is an essential pro-steatotic stimulus and a potential therapeutic target for fibrosis management [4,5]. In addition, recent evidence indicates that enoyl coenzyme A hydratase 1 (ECH1) is a key component in mitochondrial fatty acid β-oxidation, and its overexpression not only alleviates inflammation and fibrogenesis but also alleviates oxidative stress [6,7].

Carrimycin (CAR), a new genetic engineering 16-membered macrolide antibiotic, containing a group of 4″-acylated spiramycins with three 4″*O*-isovalerylspiramycins major components (ISP I, II, and III) [8,9]. Previous studies showed that carrimycin and ISP I could inhibit growths of hepatocellular carcinoma [10]. In our efforts to search for fibrotic candidates, carrimycin was selected for

* Corresponding author.
** Corresponding author.
E-mail addresses: heweiqing@imb.pumc.edu.cn (W. He), hehwei@imb.pumc.edu.cn (H. He).
Peer review under responsibility of Xi'an Jiaotong University.
[1] Both authors contributed equally to this work.

https://doi.org/10.1016/j.jpha.2024.101048

further investigation as one of the most active [11,12]. ISP I as one of the major components was proved to acquire a similar inhibition on the *COL1A1* promoter. Therefore, it is worthy to evaluate the activities and mechanisms of ISP I in protecting against liver injury and liver fibrosis.

Vascular non-inflammatory molecule-1 (Vanin-1, VNN1), as a glycosylphosphatidyl inositol (GPI)-anchored pantetheinase, is reported highly expressed in the liver and serves as an oxidative stress sensor [13]. It can catalyze the hydrolysis of D-pantetheine in the dissimilative pathway of CoA and the acyl carrier protein, thus permitting the recycling of pantothenate and the generation of cysteamine [14]. Moreover, cysteamine can promote the transport of cysteine into cells, which can be further used to synthesize glutathione (GSH), one of the most potent intracellular antioxidants [15]. Importantly, the free cysteamine level strictly correlates to the presence of membrane-bound VNN1 [16].

Iron-sulfur (Fe—S) clusters are among the oldest cofactors and have been proposed to have a critical role in the emergence of life [17,18]. [2Fe—2S] and [4Fe—4S] clusters are the most commonly found in biological systems, and [4Fe—4S] clusters are first assembled on the cytosolic iron-sulfur cluster assembly (CIA) scaffold complex composed of nucleotide-binding protein 1 (NUBP1) and nucleotide-binding protein 2 (NUBP2) [19,20]. Our research indicated that NUBP2 might be the direct target of ISP I. However, there are few reports of NUBP2 at present, to reveal how NUBP2 regulates liver fibrosis and its detailed action on ISP I is especially inventive.

In all, we aim to evaluate the function and mechanism of ISP I in the protection against liver injury and liver fibrosis *in vivo* and *in vitro*. In addition, the activity of carrimycin against liver injury and liver fibrosis will be determined simultaneously. After elaborate investigation, our study reveals ISP I or carrimycin might be a novel candidate for liver fibrosis, and the NUBP2-VNN1 pathway plays an essential role in exerting its pharmacological activity.

2. Methods

2.1. Chemicals and reagents

Human hepatic stellate cell line LX-2 and macrophage THP-1 were purchased from the Cell Resource Center of Peking Union Medical College (Beijing, China). The recombined protein transforming growth factor beta 1 (TGF-β1) was obtained from R&D Systems (Minneapolis, MN, USA). Antibodies against α-SMA, TGF-β1, and COL1A1 antibodies were bought from Abnova (Walnut, CA, USA). Antibody against tissue inhibitor of metalloproteinases 1 (TIMP1) was purchased from Proteintech (Wuhan, China). Antibodies against nuclear factor-kappaB (NF-κB) p65 and p-NF-κB p65 were purchased from Santa Cruz Biotechnology (Santa Cruz, CA, USA). All the other antibodies were purchased from Cell Signaling Technology (Beverley, MA, USA). The real-time polymerase chain reaction (PCR) master mix was purchased from Roche (Indianapolis, IN, USA). ABI TaqMan primers were purchased from Applied Biosystems (Foster City, CA, USA). Shen Yang Tonglian Group (Shenyang, China) provided carrimycin. ISP I was isolated and purified from carrimycin, and its purity >99.9% was detected by high-performance liquid chromatography (HPLC). The ISP I-Biotin was synthesized by Xi'an Qiyue Biological Technology (Xi'an, China).

2.2. Cell culture and treatment

The LX-2 cells were cultured in Dulbecco's modified Eagle medium (DMEM)/GlutaMAX (Gibco, Waltham, MA, USA) and THP-1 cells were cultured in RPMI1640 medium (Hyclone, Logan, UT, USA). All the cells were supplemented with 10 % fetal bovine serum (FBS; Hyclone), and 1 % penicillin/streptomycin (Hyclone) at 37 °C in 5 % CO_2.

LX-2 cells were starved for 24 h when the cells reached 70 %—80 % confluence. After that, the TGF-β1 group was induced by TGF-β1 (2 ng/mL) for another 24 h, and the ISP I or CAR group was added to different concentrations of ISP I or carrimycin together with TGF-β1.

THP-1 cells were differentiated by phorbol 12-myristate 13-acetate (PMA; 50 ng/mL) for 24—48 h first and then pretreated with ISP I (10 μM, and 20 μM) for 4 h. After that, the cells were followed by lipopolysaccharides (LPS; 1 μg/mL) stimulation for 3 h and nigericin (5 μM) for another 30 min. The proteins were collected in the supernatant and the whole cell lysate (WCL).

2.3. Bile duct ligation (BDL) rats' model

Male Sprague-Dawley (SD) rats, weighing 180—200 g, were used for this study. The sham-operated group was the control. The BDL, BDL-ISP I, or BDL-CAR groups all received BDL surgery [21]. The BDL-ISP I group was intragastric administrated with ISP I (100 mg/kg) once a day for 14 days. The BDL-CAR group was intragastric administrated with carrimycin (100 mg/kg) once a day for 14 days. After treatment, all rats were euthanized in random order after an overnight fast. Urine samples were collected after overnight fasting using a metabolic cage. Serum and liver samples were collected for further analysis.

2.4. Carbon tetrachloride (CCl_4) mice model

Eight-week-old male C57BL/6 N mice were fed a normal chow diet (ND) or Western diet (WD) (TD. 120528, Teklad diets) containing 21.1% fat, 41% sucrose, 1.25% cholesterol, and a high sugar solution. CCl_4 (0.2 μL/g) was injected intraperitoneally weekly for 14 weeks [22]. Experimental groups were as follows: Oil (ND/oil), CCl_4 (WD/CCl_4), and CCl_4-ISP I (WD/CCl_4/ISP I). For the last four weeks, the CCl_4-ISP I group was intragastric administrated with ISP I (100 mg/kg) once a day.

2.5. Multiple drug resistance (Mdr2)-KO mice model

Eight-week-old male Mdr2-KO (FVB.129P2-*Abcb4*^{tm1Bor}/J) mice were purchased from the Jackson Laboratory (Sacramento, CA, USA), and wild-type (WT) in FVB/NJ background was used as control [23]. The experiment groups were as follows: WT (WT), Model (Mdr2-KO), and CAR (Mdr2-KO/CAR). CAR group was intragastric administrated with carrimycin (100 mg/kg) once a day for 4 weeks, the WT group and Model group were administrated with saline as the controls. Finally, all the mice were euthanized and liver and serum samples were collected.

2.6. Animal experiments statement

All the animal experiments were performed in compliance with the ARRIVE guidelines 2.0 and institutional guidelines of the Institute of Medicinal Biotechnology, Chinese Academy of Medical Sciences (Approval number: IMB-20221230D201).

2.7. Serum and urine biochemistry

Serum alanine aminotransferase (ALT), aspartate aminotransferase (AST), lactate dehydrogenase (LDH), alkaline phosphatase (ALP), total bile acid (TBA), total bilirubin (TBiL), γ-glutamyl transpeptidase (γ-GT), high-density lipoprotein (HDL), as well as TBiL and TBA in urine were analyzed using a Hitachi 7170 chemistry analyzer with kits from Zhongsheng Beikong Biotechnology (Beijing, China).

2.8. Liver histology and hydroxyproline content determination

Formalin-fixed, paraffin-embedded liver sections were stained for assessment of liver histology. 5 μm sections were stained with hematoxylin and eosin (H&E) staining, Sirius red staining, and Masson staining. Two expert pathologists who performed a histological evaluation of the liver sections assessed for bile duct proliferation, necrosis, and inflammation on a 5-point scale (A0–5) [24,25]. Sirius red- or Masson-stained sections were photographed and used ImageJ to quantify the positive area density [25]. The hydroxyproline content in liver tissue was determined by alkaline hydrolysis. The obtained liver tissues were homogenized on ice, and centrifuged, and the supernatant was collected. The hydroxyproline content in the supernatant was analyzed using a hydroxyproline colorimetric assay kit (A301–2–1, Nanjing Jiancheng, Nanjing, China) according to the manufacturer's instructions.

2.9. Western blot

Cells or liver tissues were homogenized in radioimmunoprecipitation assay (RIPA) buffer and then centrifuged at 12,000 rpm for 15 min at 4 °C. Equal amounts of lysate were mixed with 5 × sodium dodecyl sulfate (SDS) loading buffer resolved by sodium dodecyl sulfate-polyacrylamide gel electrophoresis (SDS-PAGE) and transferred to a polyvinylidene fluoride (PVDF) membrane (Millipore, MA, USA). The membranes were blocked with 5 % non-fat milk in Tris-buffered saline with Tween-20 (TBS-T) buffer at room temperature for 1 h and then incubated with primary antibodies at 4 °C overnight. The membranes were incubated with an appropriate horseradish peroxidase (HRP)-conjugated secondary antibody for 1 h at room temperature, and then the images were captured by an exposure instrument.

2.10. Co-immunoprecipitation (Co-IP) analysis

The LX-2 cells were homogenized into IP-specific lysis buffer (Thermo Scientific, Waltham, MA, USA) at 4 °C for 30 min, followed by centrifugation at 12,000 rpm for 15 min. The cell lysates were then collected and incubated with protein A/G magnetic agarose beads (Thermo Scientific) at room temperature with mixing for 1–2 h, and were subsequently co-incubated with the indicated antibodies at 4 °C overnight. After rinsing with washing buffer 3 times, the immune complex was collected and subjected to Western blot analysis.

2.11. Determination of cysteamine, GSH, and malondialdehyde (MDA) levels

Cysteamine level was detected through HPLC according to previous methods [26,27]. LX-2 cells were washed twice in warm Hank's balanced salt solution and immediately lysed with 100 μL lysis buffer. Thereafter, 15 μL of 0.1 M HCl and 140 μL of precipitating solution were added. After centrifugation at 12,000 rpm for 10 min, the supernatants were collected, and 25% (*v*/*v*) Na_2HPO_4

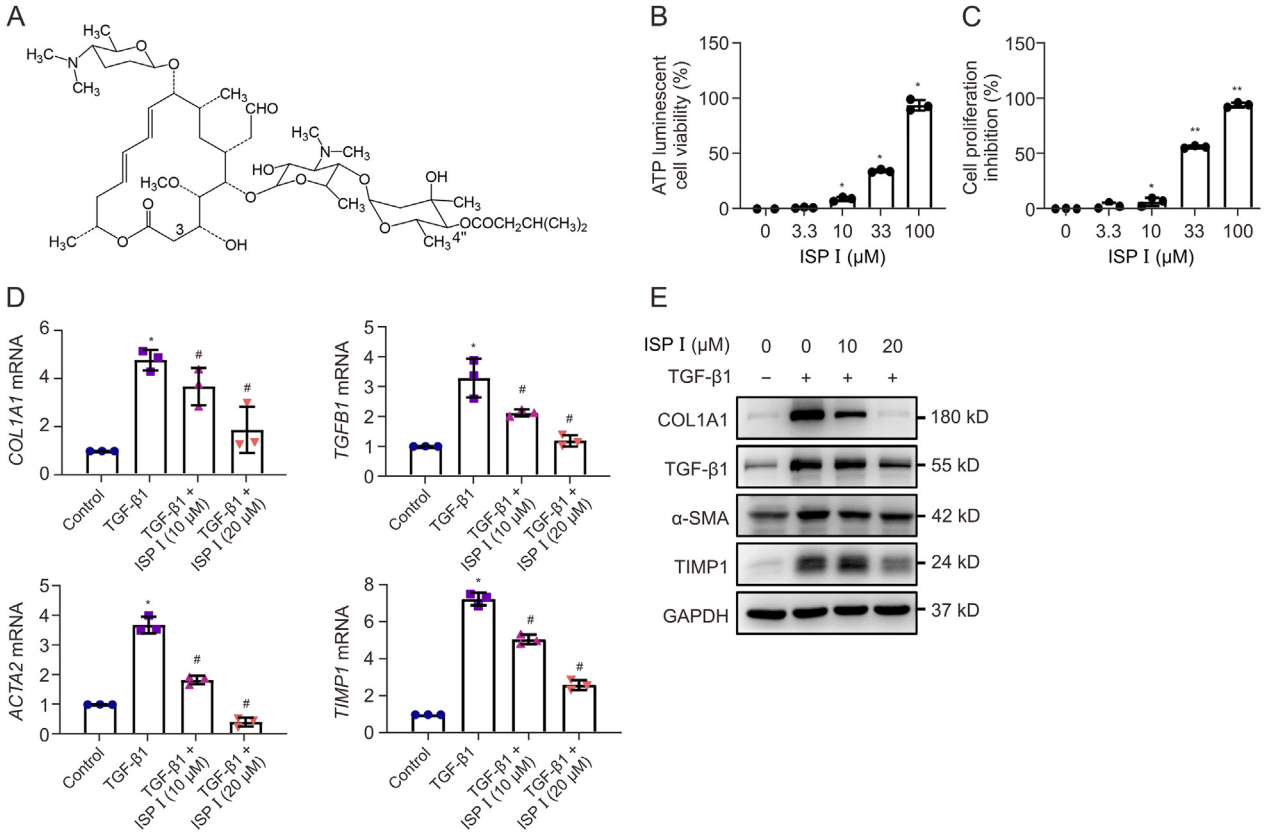

Fig. 1. Inhibitory effects of isovalerylspiramycin I (ISP I) on cell viability and fibrogenic biomarkers. (A) The chemical structure of ISP I. (B, C) LX-2 cells were treated with the indicated concentrations of ISP I (3.3, 10, 33, and 100 μM) of ISP I for 48 h. The cell viability was measured by ATP luminescent cell viability assay (B) or sulforhodamine B (C). The values were expressed as the mean ± standard error of the mean (SEM). $n = 3$, $^{*}P < 0.05$, $^{**}P < 0.01$ vs. 0 μM. (D, E) LX-2 cells were starved for 24 h, followed by treatment with transforming growth factor beta 1 (TGF-β1; 2 ng/mL) and ISP I (10, and 20 μM) for another 24 h. Quantitative reverse transcription polymerase chain reaction (qRT-PCR) analysis of *collagen type I alpha 1 (COL1A1)*, *TGFB1*, *Actin alpha 2 (ACTA2)*, and *tissue inhibitors of metalloproteinase 1 (TIMP1)* mRNA levels. The values were expressed as mean ± SEM. $n = 3$, $^{*}P <$ 0.05 vs. control group, and $^{\#}P < 0.05$ vs. TGF-β1 group (D). Western blot analysis of COL1A1, TGF-β1, alpha-smooth muscle actin (α-SMA), and TIMP1 protein expressions (E). GAPDH: glyceraldehyde-3-phosphate dehydrogenase.

and immediately after 10% (*v*/*v*) 5,5'-dithiobis-(2-nitrobenzoic acid) (DTNB) were added. The mixture was stirred for 1 min, then it was left for another 5 min at room temperature. Finally, HPLC was used for cysteamine determination.

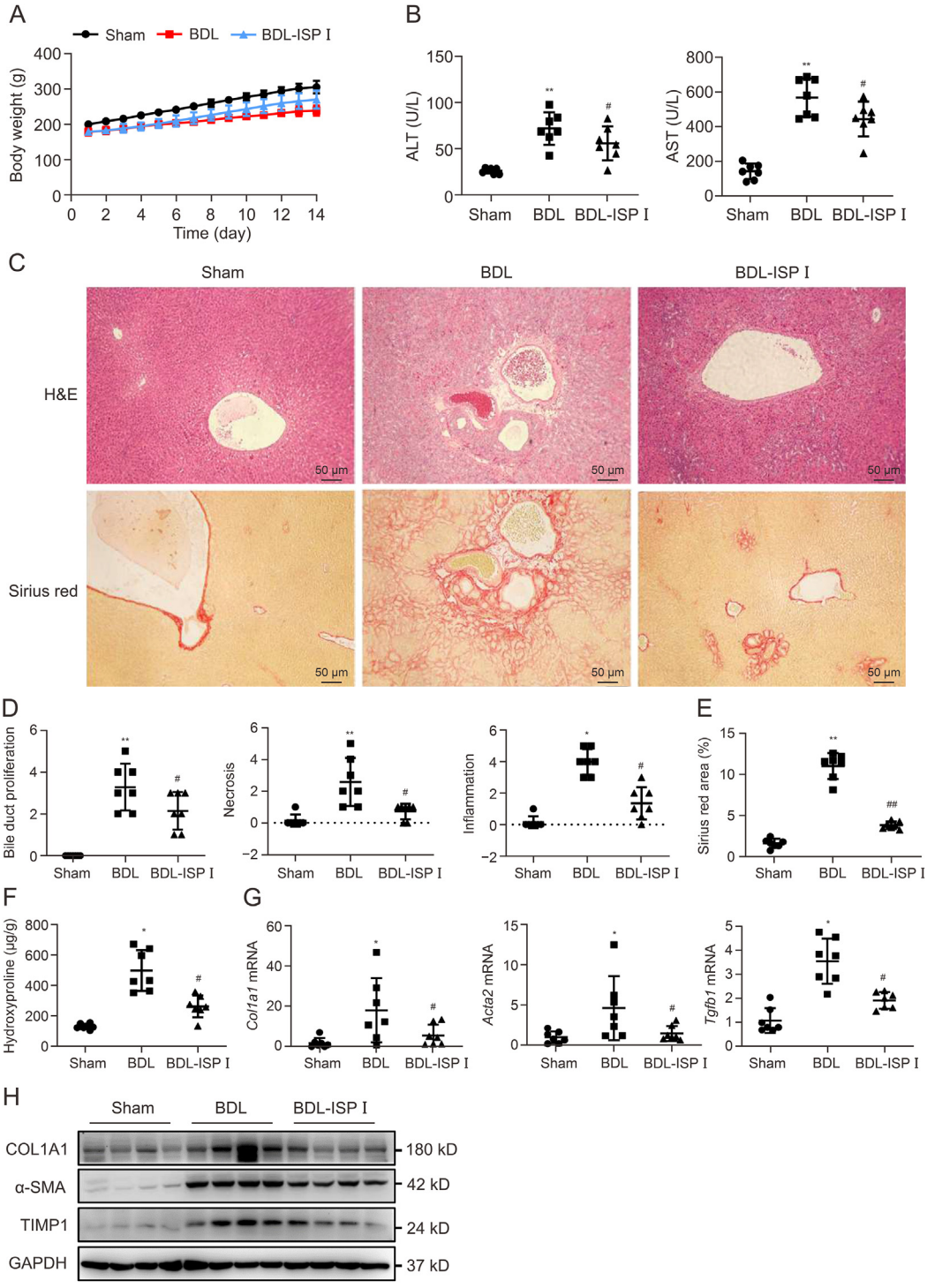

Fig. 2. Amelioration effects of isovalerylspiramycin I (ISP I) on bile duct ligation (BDL)-induced liver damage and liver fibrosis in Sprague-Dawley (SD) rats. Male SD rats underwent BDL operation and oral administration with ISP I (100 mg/kg) for 14 days. (A) The body weight during the 14 days. (B) The levels of alanine aminotransferase (ALT) and aspartate aminotransferase (AST) in serum. (C) Representative histological images of hematoxylin and eosin (H&E)- and Sirius red-stained liver sections. (D) Blinded quantitative assessment of bile duct proliferation, necrosis, and inflammation in H&E-stained livers. (E) Quantitative measurement of positive area in Sirius red-stained livers. (F) Hydroxyproline level in livers. (G) Quantitative reverse transcription polymerase chain reaction (qRT-PCR) analysis of *collagen type 1 alpha 1* (*Colla1*), *Actin Alpha 2* (*Acta2*), *and transforming growth factor beta 1* (*Tgfb1*) mRNA levels in liver samples. (H) Western blot analysis of COL1A1, alpha-smooth muscle actin (α-SMA), and tissue inhibitors of metalloproteinase 1 (TIMP1) expressions in liver samples. Data were expressed as mean ± standard error of the mean (SEM). $n = 7$, $^{*}P < 0.05$, $^{**}P < 0.01$ vs. sham group, and $^{\#}P < 0.05$, $^{\#\#}P < 0.01$ vs. BDL group. GAPDH: glyceraldehyde-3-phosphate dehydrogenase.

LX-2 cells were washed with PBS and then homogenized on ice. After centrifugating at 12,000 rpm for 15 min at 4 °C, the supernatants were harvested. The GSH level was detected using a micro-reduced GSH assay kit (Solarbio, Beijing, China), and the malondialdehyde (MDA) level was assessed using an assay kit (Beyotime, Shanghai, China).

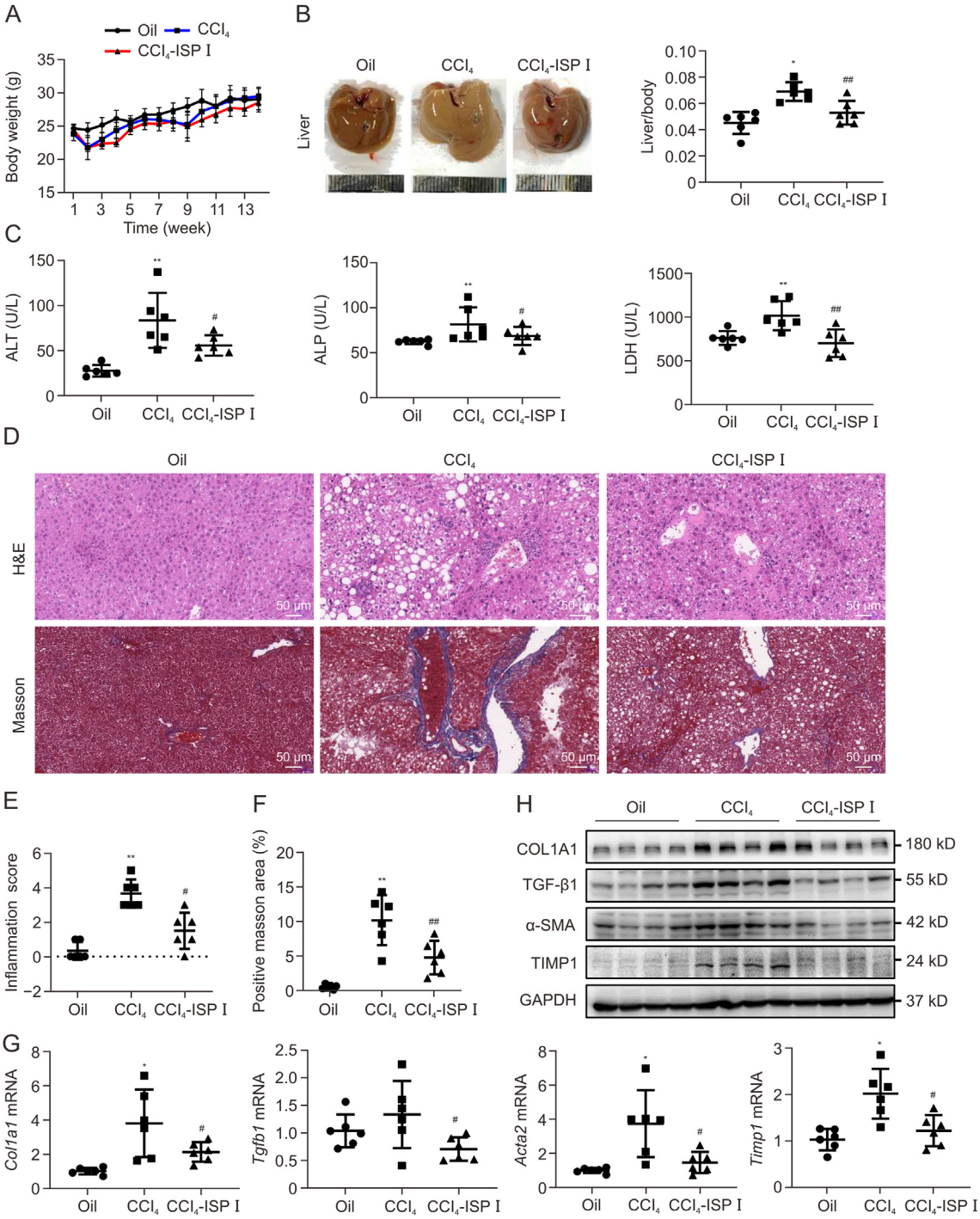

Fig. 3. Amelioration effects of isovalerylspiramycin I (ISP I) on CCl_4-induced liver damage and liver fibrosis in C57BL/6 N mice. C57BL/6 N mice were intra-peritoneal injected with CCl_4 (0.2 μL/g) once a week for 14 weeks. The CCl_4-ISP I group was administrated with ISP I (100 mg/kg) for the last 4 weeks. (A) The body weight. (B) Representative pictures of the livers and liver-to-body ratio. (C) The levels of alanine aminotransferase (ALT), alkaline phosphatase (ALP), and lactate dehydrogenase (LDH) in serum. (D) Representative histological images of hematoxylin and eosin (H&E)- and Masson-staining. (E) The score of inflammation. (F) Quantitative measurement of positive brown areas. (G) Quantitative reverse transcription polymerase chain reaction (qRT-PCR) analysis of *collagen type 1 alpha 1* (*Colla1*), *transforming growth factor beta 1* (*Tgfb1*), *Actin Alpha 2* (*Acta2*), *transforming growth factor beta 1* (*Tgfb1*), and *tissue inhibitors of metalloproteinase 1* (*Timp1*) levels. Data were expressed as mean ± standard error of the mean (SEM). $n = 6$, $^{*}P < 0.05$, $^{**}P < 0.01$ vs. Oil group, and $^{\#}P < 0.05$, $^{\#\#}P < 0.01$ vs. CCl_4 group. (H) Western blot analysis of COL1A1, TGF-β1, alpha-smooth muscle actin (α-SMA), and TIMP1 expressions in liver samples. GAPDH: glyceraldehyde-3-phosphate dehydrogenase.

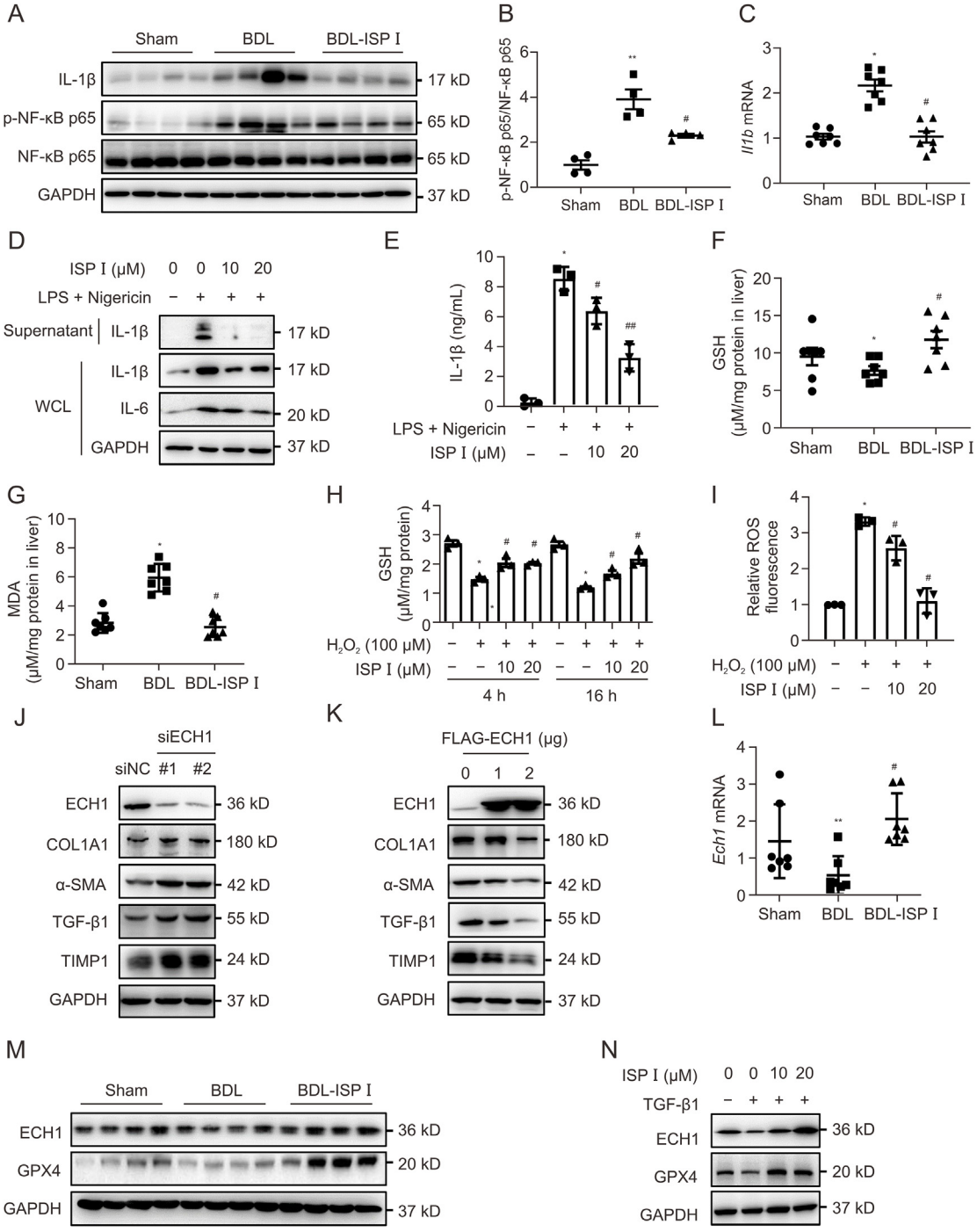

Fig. 4. Isovalerylspiramycin I (ISP I) alleviated the inflammation and oxidation stress. (A, B) Extracting the total proteins in bile duct ligation (BDL) rat livers, and Western blot analysis of interleukin-1 beta (IL-1β), p-nuclear factor-kappaB (NF-κB) p65, and NF-κB p65 (A); quantifying the density, the ratio of p-NF-κB p65/NF-κB p65 is calculated (B). (C) Extracting the RNA in BDL rat livers, and quantitative reverse transcription polymerase chain reaction (qRT-PCR) analysis of *Il1b*. (D, E) THP-1 cells were pretreated with ISP I (10, and 20 μM) for 4 h, followed by lipopolysaccharides (LPS; 1 μg/mL) stimulation for 3 h and nigericin (5 μM) for another 30 min. IL-1β in the supernatant and IL-1β, and IL-6 in the whole cell lysate (WCL) were determined (D); IL-1β in the supernatant was determined by enzyme-linked immunosorbent assay. Data were expressed as mean ± standard error of the mean (SEM). $n = 3$, $^{*}P < 0.05$ vs. non-treated group, and $^{\#}P < 0.05$, $^{\#\#}P < 0.01$ vs. LPS + Nigericin group (E). (F, G) Glutathione (GSH) (F) and malondialdehyde (MDA) (G) activity in BDL rat livers. $n = 7$, $^{*}P < 0.05$ vs. sham group, and $^{\#}P < 0.05$ vs. BDL group. (H) LX-2 cells were treated by H_2O_2 (100 μM) and ISP I (10, and μM) for 4 h or 16 h. The GSH level was detected. $n = 3$, $^{*}P < 0.05$ vs. non-treated group, and $^{\#}P < 0.05$ vs. H_2O_2 group. (I) LX-2 cells were activated by H_2O_2 (100 μM) for 3 h and followed by ISP I (10, and 20 μM) treatment simultaneously, the reactive oxygen species (ROS) fluorescence was measured. $n = 3$, $^{*}P < 0.05$ vs. non-treated group, and $^{\#}P < 0.05$ vs. H_2O_2 group. (J, K) LX-2 cells were transfected with siECH1 (J) or FLAG-ECH1 (K) for 48 h. Western blot analysis of enoyl coenzyme A hydratase 1 (ECH1), collagen type I alpha 1 (COL1A1), transforming growth factor beta 1 (TGF-β1), alpha-smooth muscle actin (α-SMA), and tissue inhibitors of metalloproteinase 1 (TIMP1). (L) Quantitative reverse transcription polymerase chain reaction (qRT-PCR) analysis of *Ech1* mRNA level in BDL livers. $n = 7$, $^{**}P < 0.01$ vs. sham group, and $^{\#}P < 0.05$ vs. BDL group. (M) Western blot analysis of ECH1 and glutathione peroxidase 4 (GPX4) protein levels in BDL rat livers. (N) LX-2 cells were starved and treated with TGF-β1 (2 ng/mL) combined with ISP I (10, and 20 μM) for 24 h. Western blot analysis of ECH1 and GPX4. siNC: small interfering RNA negative control; GAPDH: glyceraldehyde-3-phosphate dehydrogenase.

2.12. Cellular thermal shift assay (CETSA)

LX-2 cells at 80 %–90 % confluence were treated with ISP I (40 μM) or dimethyl sulfoxide (DMSO) for 3 h. Then the cells were harvested and the suspension was incubated at each temperature point from 37 °C to 57 °C for 3 min. After the samples were freeze-thaw 3 times and centrifuged at 12,000 rpm at 4 °C for 10 min, the samples were separated by SDS-PAGE.

2.13. Statistical analysis

GraphPad Prism 9.0 software was used for statistical analysis. All experiments were performed at least thrice, and the results were expressed as mean ± standard error of the mean (SEM) where applicable. One-way analysis of variance (ANOVA) or a two-tailed Student's *t*-test was performed to analyze the statistical significance. The value of $P < 0.05$ was considered statistically significant.

3. Results

3.1. ISP I inhibited the viability and fibrogenic gene expressions in human LX-2 cells

The inhibition effect of ISP I (Fig. 1A) on LX-2 was determined by sulforhodamine B (SRB) assay and ATP luminescent cell viability assay (YEASEN Biotechnology, Shanghai, China). ISP I inhibited LX-2 proliferation and activity significantly above the concentration of 10 μM (Figs. 1B and C). Subsequently, the influence of ISP I on fibrogenic genes was detected. ISP I dose-dependently downregulated expressions of various markers, including *COL1A1*, *ACTA2*, *TGFB1*, and *TIMP1* (Figs. 1D and E). These

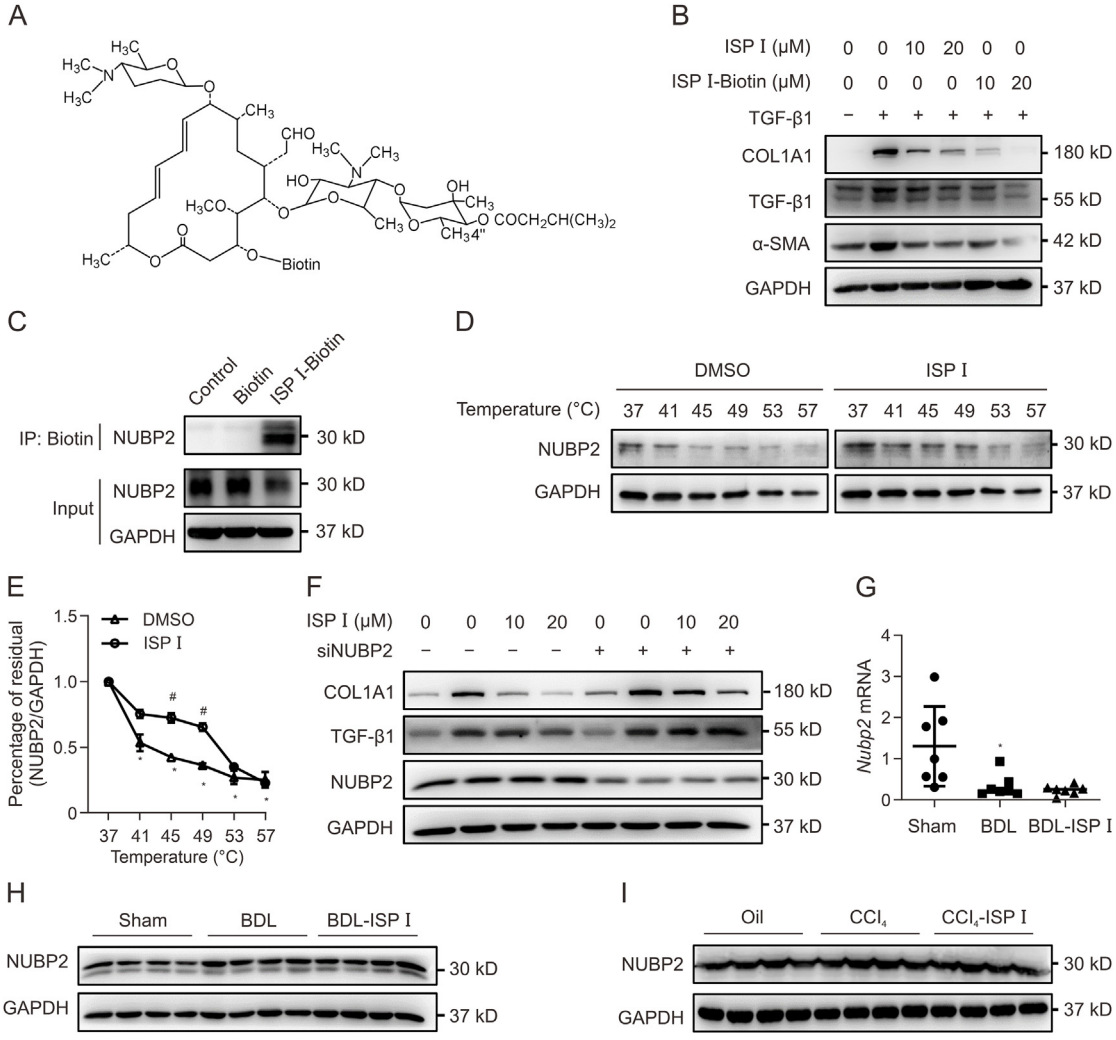

Fig. 5. The identification of the target protein of isovalerylspiramycin I (ISP I). (A) Chemical structure of ISP I-Biotin probe. (B) LX-2 cells were starved for 24 h, followed by treatment with transforming growth factor beta 1 (TGF-β1) (2 ng/mL) combined with ISP I (10, and 20 μM) or ISP I-Biotin (10, and 20 μM) for 24 h. Western blot analysis of collagen type I alpha 1 (COL1A1), transforming growth factor beta 1 (TGF-β1), and alpha-smooth muscle actin (α-SMA). (C) LX-2 cells were treated with ISP I-Biotin or Biotin for 12 h, and then the cell lysis was pulled down with protein A/G beads. Nucleotide-binding protein 2 (NUBP2) in the complex was analyzed. (D, E) Cellular thermal shift assay of NUBP2 (D); and the statistical plots (E). $n = 3$, $^{*}P < 0.05$ vs. 37 °C of dimethyl sulfoxide (DMSO) group, and $^{\#}P < 0.05$ vs. ISP I group. (F) LX-2 cells were transfected with siNUBP2 for 48 h, then treated with ISP I or DMSO for another 24 h. Western blot analysis of COL1A1, TGF-β1, and NUBP2. (G) Quantitative reverse transcription polymerase chain reaction (qRT-PCR) analysis of *Nubp2* mRNA level in the livers of bile duct ligation (BDL) model. $n = 7$, $^{*}P < 0.05$ vs. sham group. (H) Western blot analysis of NUBP2 in the livers of BDL model. (I) Western blot analysis of NUBP2 in the livers of the CCl_4 model. GAPDH: glyceraldehyde-3-phosphate dehydrogenase.

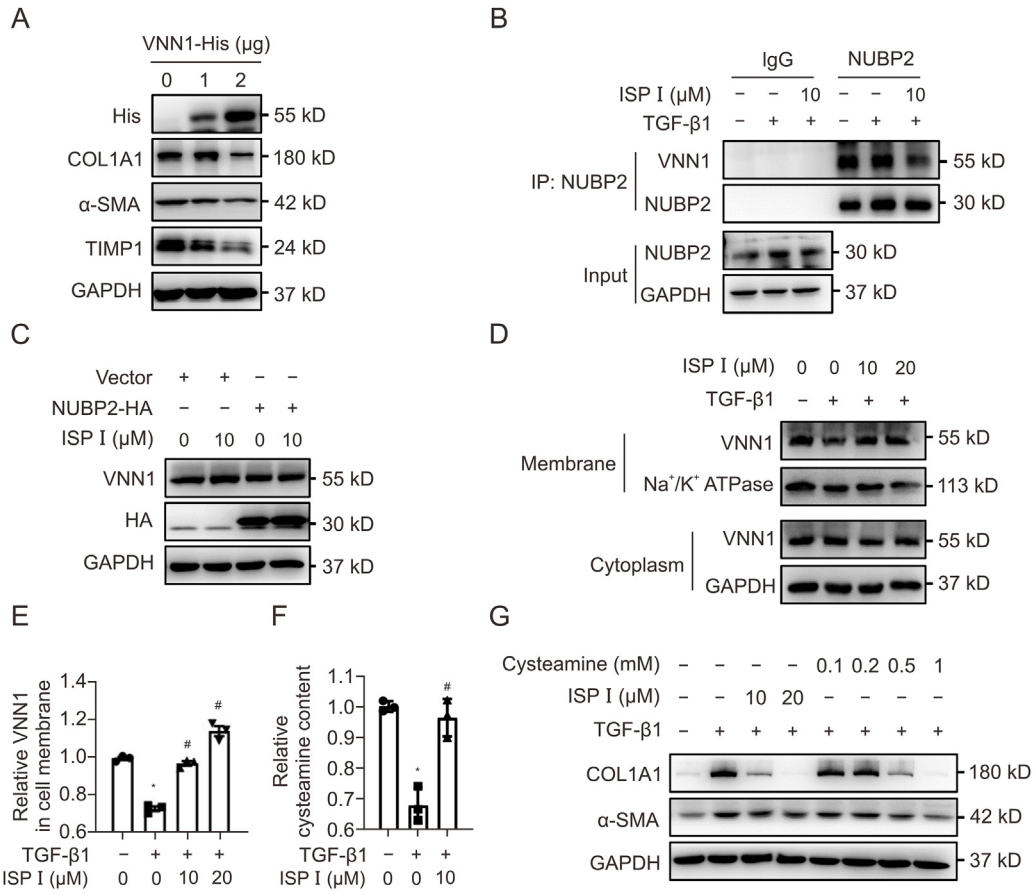

Fig. 6. Isovalerylspiramycin I (ISP I) increased vascular non-inflammatory molecule-1 (VNN1) activity by reducing its interaction with nucleotide-binding protein 2 (NUBP2). (A) LX-2 cells were transfected with VNN1-His plasmid for 48 h, and then treated with transforming growth factor beta 1 (TGF-β1; 2 ng/mL) for another 24 h. The expressions of VNN1, collagen type I alpha 1 (COL1A1), alpha-smooth muscle actin (α-SMA), and tissue inhibitors of metalloproteinase 1 (TIMP1) were measured. (B) TGF-β1-stimulated LX-2 cells were treated with ISP I (10 μM) for 24 h, and then the cells were lysed in an immunoprecipitation lysis buffer. One part was incubated with IgG, and another part with NUBP2. The proteins pulled down were immunoblotted with VNN1 and NUBP2. (C) LX-2 cells were transfected with NUBP2-HA for 48 h and then treated with ISP I (10 μM) for 24 h. The expressions of VNN1 andHA tag were analyzed. (D) TGF-β1-stimulated LX-2 cells were treated with ISP I (10, and 20 μM) for 24 h, and then the components in the cell membrane and cytoplasm were separated. VNN1 in the cell membrane and cytoplasm were detected, with Na^+/K^+ ATPase and glyceraldehyde-3-phosphate dehydrogenase (GAPDH) as the internal controls, respectively. (E) VNN1 in the cell membrane was calculated by gray scanning and normalized to Na^+/K^+ ATPase. (F) The cysteamine content in LX-2 cells induced by TGF-β1 and ISP I (10 μM). $n = 3$, $^*P < 0.05$ vs. non-treated group, and $^\#P < 0.05$ vs. TGF-β1 group. (G) TGF-β1-stimulated LX-2 cells were treated with ISP I (10, and 20 μM) or cysteamine (0.1, 0.2, 0.5, and 1 mM) for 24 h, and then COL1A1 and α-SMA were detected.

results indicated that ISP I could serve as a potent anti-fibrogenic agent in the future.

3.2. ISP I protected against BDL-induced liver injury and liver fibrosis in SD rats

We investigated the *in vivo* biological activity of ISP I in the BDL model. Results showed that weight gain in the BDL-ISP I group was higher than that in the BDL group, indicating the lower toxicity of ISP I *in vivo* (Fig. 2A). Besides, significant reductions in ALT and AST levels were observed in the BDL-ISP I group (Fig. 2B). H&E staining demonstrated that the histological liver structure in the BDL group was severely damaged, paralleled by newly formed bile ducts and concomitant extensive parenchyma necrosis, as well as inflammation (Fig. 2C, up panel). ISP I administration substantially improved these pathological changes by double-blinded assessment (Fig. 2D).

Synchronously, we evaluated the anti-fibrotic effect of ISP I by Sirius red staining and hydroxyproline content detection. In BDL rats, Sirius red-stained collagen fibrils extended to not only the portal areas but also the hepatic parenchyma, and this effect was markedly attenuated by ISP I treatment (Figs. 2C and E). Additionally, ISP I dramatically reduced the BDL-induced hydroxyproline content (Fig. 2F). To further verify the anti-fibrotic activity of ISP I, we measured the expression of fibrogenic markers in the livers. The mRNA levels including *Col1a1*, *Acta2*, and *Tgfb1* were all repressed by ISP I treatment (Fig. 2G), and the protein levels of COL1A1, α-SMA, and TIMP1 were markedly reduced (Fig. 2H). These results revealed that ISP I treatment attenuated liver damage and repressed fibrogenic gene expressions in BDL rats.

3.3. ISP I protects against CCl_4-induced liver injury and fibrosis in C57BL/6 N mice

CCl_4 has been widely used for decades to induce liver injury and fibrosis in mice. Fig. 3A indicated that CCl_4 or ISP I treatment did not induce a significant difference in weight gain up to 14 weeks. Whereas the CCl_4 group developed an increased liver-to-body ratio, and the parameter significantly decreased in the CCl_4-ISP I group (Fig. 3B). In contrast to the CCl_4 group, CCl_4-ISP I decreased ALT, ALP, and LDH significantly (Fig. 3C). In addition, H&E staining showed the protective effect of ISP I on pathology and lobular inflammation (Figs. 3D and E). Quantitative morphometry assessment of fibrotic tissue area showed there was a decreased trend towards collagen

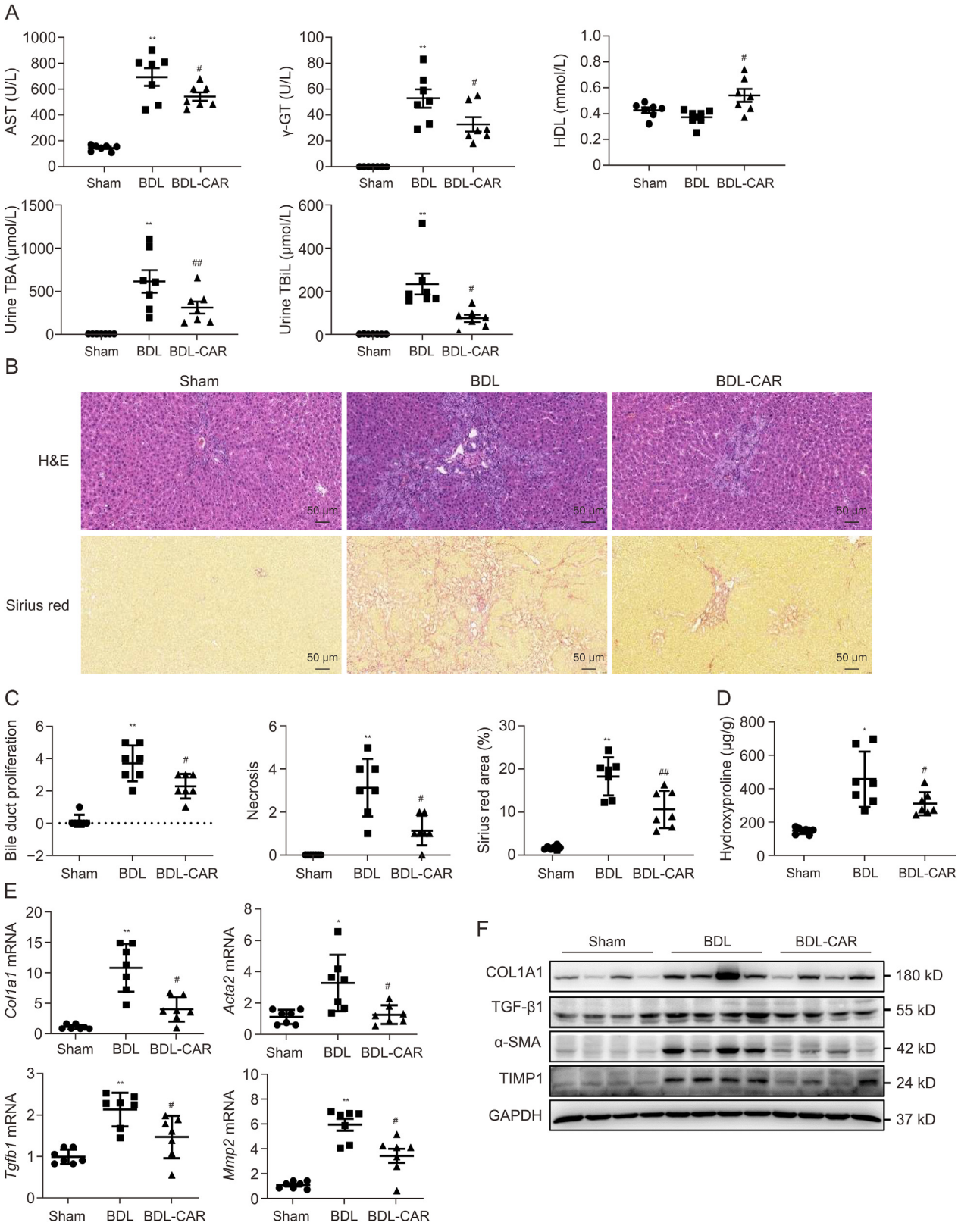

Fig. 7. Anti-liver fibrosis and liver-protective effects of carrimycin (CAR). Male Sprague-Dawley (SD) rats undergoing bile duct ligation (BDL) operation were orally administered carrimycin (100 mg/kg) for 14 days. (A) The levels of aspartate aminotransferase (AST), γ-glutamyl transpeptidase (γ-GT) and high-density lipoprotein (HDL) in serum, and total bile acid (TBA) and total bilirubin (TBiL) in urine. (B) Representative histological images of hematoxylin and eosin (H&E)- and Sirius red-stained liver sections. (C) Blinded quantitative assessment of bile duct proliferation and necrosis in H&E-stained livers, and quantitative measurement of positive area in Sirius red-stained livers. (D) Hydroxyproline level. (E) Quantitative reverse transcription polymerase chain reaction (qRT-PCR) analysis of *collagen type 1 alpha 1* (*Colla1*), *Actin Alpha 2* (*Acta2*), *transforming growth factor beta 1* (*Tgfb1*), and *matrix metalloproteinase 2* (*Mmp2*) mRNA levels in liver samples. (F) Western blot analysis of COL1A1, TGF-β1, alpha-smooth muscle actin (α-SMA), and tissue inhibitors of metalloproteinase 1 (TIMP1) expressions in liver samples. $n = 7$, $^{*}P < 0.05$, $^{**}P < 0.01$ vs. sham group; $^{\#}P < 0.05$, $^{\#\#}P < 0.01$ vs. BDL group. GAPDH: glyceraldehyde-3-phosphate dehydrogenase.

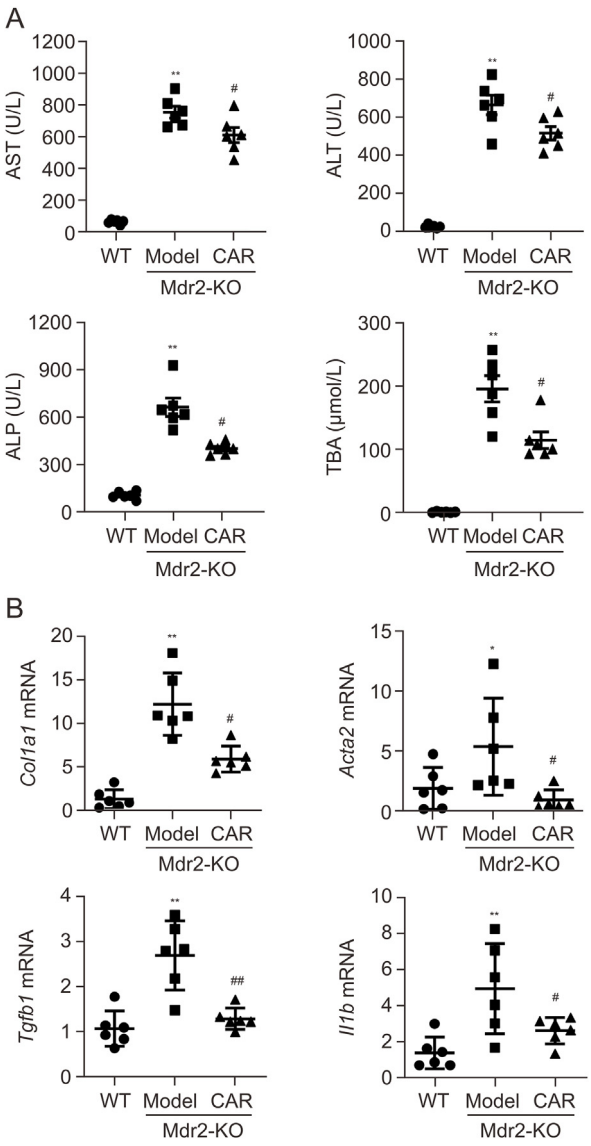

Fig. 8. Liver-protective and anti-liver fibrosis effects of carrimycin (CAR) in multiple drug resistance (Mdr2)-KO mice. (A) The aspartate aminotransferase (AST), alanine aminotransferase (ALT), alkaline phosphatase (ALP), and total bile acid (TBA) levels in serum. (B) Quantitative reverse transcription polymerase chain reaction (qRT-PCR) analysis of *collagen type 1 alpha 1* (*Colla1*), *Actin Alpha 2* (*Acta2*), *transforming growth factor beta 1* (*Tgfb1*), and *interleukin-1 beta* (*Il1b*) mRNA levels in liver samples. Data were expressed as mean ± standard error of the mean (SEM). $n = 6$, $^{*}P < 0.05$, $^{**}P < 0.01$ vs. WT group, and $^{\#}P < 0.05$, $^{\#\#}P < 0.01$ vs. Model group. WT: wild type mice.

deposition in ISP I mice (Figs. 3D and F). Quantitative reverse transcription polymerase chain reaction (qRT-PCR) and Western blot confirmed that upregulated fibrogenic genes such as *Col1a1*, *Tgfb1*, *Acta2*, and *Timp1* by CCl_4 treatment were reversed by ISP I administration (Figs. 3G and H).

3.4. Anti-inflammation and anti-oxidation activity of ISP I

Inflammation and oxidation as the notable predisposition of liver injury, their severe progression was measured in BDL rats. Firstly, the notable downregulation of IL-1β suggested that ISP I could reduce inflammatory reactions (Figs. 4A and C). The repressed p-NF-κB p65 confirmed ISP I inhibited NF-κB mediated inflammatory pathway (Figs. 4A and B). Later, the effect of ISP I on IL-1β was investigated in THP-1 cells. As anticipated, ISP I greatly diminished mature IL-1β production to an undetected level (Fig. 4D). Interestingly, ISP I also decreased the levels of IL-1β and IL-6 in the WCL (Fig. 4D). Meanwhile, Enzyme-linked immunosorbent assay also proved the repressive activity of ISP I in THP-1 cells (Fig. 4E). These results abundantly proved the anti-inflammatory effect of ISP I and supported the idea that the liver-protective effect of ISP I may partially through inhibiting inflammasome activation.

Besides, the antioxidant molecule GSH, and the oxidative stress marker MDA, which are the main biomarkers of oxidative stress, suggested ISP I could repress oxidative stress significantly (Figs. 4F and G). In addition, the influence of ISP I in LX-2 cells was examined simultaneously. When LX-2 cells were treated with H_2O_2, GSH enzyme production was repressed. However, ISP I could reverse the inhibition of GSH production (Fig. 4H). Furthermore, ISP I also lowered the increase in harmful reactive oxygen species (ROS) caused by H_2O_2 stimulation (Fig. 4I). Moreover, by knockdown and overexpression, we confirmed the suppressor role of ECH1 in HSCs (Figs. 4J and K). ISP I could upregulate *Ech1* mRNA levels in BDL rats (Fig. 4L). Simultaneously, the increased protein expression of ECH1 and GPX4 verified the upregulation of ISP I on the ECH1 pathway (Figs. 4M and N). These results sustained the potent anti-inflammation and anti-oxidative stress activity of ISP I, and proved ISP I could increase ECH1 activity.

3.5. ISP I might perform its activity by targeting NUBP2

Next, the activity-based protein profiling (ABPP) technique was conducted to explore the direct target proteins of ISP I. According to the SAR analysis, ISP I-Biotin (Fig. 5A) was constructed. As expected, ISP I-Biotin showed equal inhibitory activity to ISP I (Fig. 5B). Afterward, the LX-2 cell lysate was divided into 2 groups, and the interacting proteins were obtained through biotin-streptavidin interaction and subsequently identified through MS analysis. Compared with the control group, five differential proteins gave high protein abundances in the ISP I-Biotin group, while undetectable levels in the biotin group (data not shown). Among them, most were cytoskeletal proteins, including the hemoglobin subunit and ribosomal protein, and only NUBP2 was reported to own catalytic activity of the Fe—S cluster. As shown in Fig. 5C, the Co-IP result indicated that only ISP I-Biotin could pull down the NUBP2 protein. Next, we performed the CETSA assay and confirmed ISP I could bond NUBP2 (Figs. 5D and E). Moreover, ISP I's activity on fibrogenic genes was weakened when knocking down NUBP2 (Fig. 5F), confirming the importance of NUBP2 for ISP I. However, ISP I did not alter the expression of NUBP2 in the BDL or CCl_4 model (Figs. 5G—I), and we conjectured that more molecules exist in the regulation of ISP I.

3.6. ISP I increased VNN1 localization on the cell membrane

The previous study showed that NUBP2 may be the target of ISP I, but how NUBP2 mediates the ISP I's activity is still unknown. In the next exploration, we found that VNN1 participated in the regulation. Overexpressing VNN1 in activated LX-2 cells repressed the expressions of fibrogenic genes including COL1A1, α-SMA, and TIMP1 (Fig. 6A). By Co-IP analysis, we found that NUBP2 can bind VNN1 protein, and their interaction could be reduced by ISP I (Fig. 6B). Therefore, ISP I may function through influencing VNN1.

However, when overexpressing NUBP2-HA or adding ISP I, the protein level of VNN1 did not change (Fig. 6C), suggesting NUBP2 or ISP I could not regulate VNN1 expression. It was reported that the membrane-bound form of VNN1 plays a general role in oxidative stress, so we separated the cell membrane and cytoplasm components in the following. Consistent with the previous studies, ISP I

increased the VNN1 that is located in the cell membrane (Figs. 6D and E). VNN1, as a pantetheinase, hydrolyzes pantetheine into pantothenic acid and cysteamine, so we also measured cysteamine content. Using HPLC, we validated increasing cysteamine content in LX-2 cells after ISP I treatment (Fig. 6F). Meanwhile, the addition of cysteamine could dose-dependently repress LX-2 activation, similar to the action of ISP I (Fig. 6G). We conclude that ISP I targets NUBP2 and inhibits the interaction of NUBP2 and VNN1, therefore increasing the localization of VNN1 in the cell membrane to release potential abilities.

3.7. CAR attenuated liver injury and fibrosis BDL rats

CAR as a multi-component bacterial fermentation product was approved for acute tracheal bronchitis and acute sinusitis in 2019. In the BDL model, the levels of serum AST, γ-GT, as well as urine TBA and urine TBiL significantly decreased after carrimycin at 100 mg/kg (Fig. 7A). Additionally, HDL increased in the carrimycin group (Fig. 7A). H&E staining demonstrated that carrimycin substantially reduced obvious bile duct proliferation and parenchyma necrosis (Figs. 7B and C). Sirius red staining results disclosed that liver collagen deposition was attenuated by carrimycin significantly (Figs. 7B and C). Meanwhile, decreased hydroxyproline levels in collagen fibers also indicated the reduced severity of hepatic fibrosis in the BDL-CAR group (Fig. 7D). qRT-PCR analysis revealed that carrimycin significantly reduced the expressions of the fibrogenic gene, including *Col1a1*, *Acta2*, *Tgfb1*, and *matrix metalloproteinase 2* (*Mmp2*) (Fig. 7E), and Western blot also confirmed the anti-fibrotic activity of carrimycin (Fig. 7F). These results indicate that carrimycin could exert an anti-fibrotic effect on the cholestatic rat model.

3.8. Carrimycin attenuated liver injury and hepatic fibrosis in Mdr2-KO mice

Deficiency of Mdr2 disrupts biliary phospholipid secretion, leading to the increase of potentially toxic bile acid, which induces hepatocyte damage and liver fibrosis. Results showed that elevations of serum ALT, AST, ALP, and TBA were found in the Model group, while these levels reduced after orally administrated with carrimycin (100 mg/kg) for 4 weeks (Fig. 8A). Furthermore, consistent with the activity in BDL rats, carrimycin exhibited well inhibition effect on the mRNA expressions of the fibrogenic gene (*Col1a1*, *Acta2*, *Tgfb1*) and pro-inflammation gene (*Il1b*) (Fig. 8B). The results confirmed the protective role of carrimycin on liver injury and hepatic fibrosis, predicting that it may be a great choice for liver fibrosis-related patients in the future.

4. Discussion

Tissue fibrosis is an excessive wound-healing response to injury, disrupting the normal tissue architecture and impairing proper organ function. In a normal liver, HSCs maintain a non-proliferative, quiescent phenotype, and become activated, *trans*-differentiation into myofibroblasts following liver injury [2]. Collagens are the most abundant ECM components in fibrosis, increasing up to tenfold in cirrhosis, especially collagen type I, III, and VI [28]. Therefore, we searched for anti-fibrosis candidates using a high-throughput drug screening cell model based on the *COL1A1* promoter [29].

In our screening, we found that carrimycin, a new genetic engineering 16-membered macrolide antibiotic, inhibited the activity of the *COL1A1* promoter significantly. Carrimycin was approved in 2019 for treating upper respiratory infections, with the advantages of low toxicity, small dosage, low frequency of administration, and convenient administration. In addition, carrimycin penetrates rat tissue well after oral medication, and high drug concentrations were observed in most organ tissue, especially in the liver [19]. Therefore, with those congenital advantages, it is meaningful to investigate carrimycin's ability to prevent or reverse fibrosis. However, due to the inclusion of nearly 20 kinds of 4″-acylated spiramycins and three 4″-*O*-isovalerylspiramycins, it is not feasible to discover the direct target and the mechanism. To avoid this contradiction, finding one univocal active compound is necessary. Therefore, by separating the ingredients, ISP I was confirmed to acquire great inhibition. Furthermore, the producing bacteria of ISP I has been constructed by our group, which makes it easy to get abundant pure ISP I in following research and commercial production [30]. Therefore, our study focused on the mechanism study of ISP I instead of carrimycin.

BDL is a well-established experimental model of cholestasis in rodents that induces a type of liver fibrosis etiologically and pathologically resembles cholestatic fibrosis in humans [31,32]. By the BDL model, the liver-protective effects of ISP I and carrimycin were proved systematically. Many biochemical markers of hepatocellular injury and cholestasis were improved, including serum ALT and AST. In addition, H&E and Sirius red or Masson staining indicated that the bile duct proliferation area and collagen deposition were markedly reduced after ISP I or carrimycin. Furthermore, the expressions of many fibrogenic genes were repressed markedly. With all the results, we concluded that ISP I and carrimycin could ameliorate liver damage and liver fibrosis in BDL rats. Beyond the BDL model, the pharmacological activity of ISP I and carrimycin was detected again in a CCl_4 model and Mdr2-KO model respectively. All these results suggest that ISP I or carrimycin might be a potent candidate for fibrosis-related diseases.

In the work of clarifying ISP I's action, its potential in reducing oxidant stress was discovered firstly. In the BDL model, ISP increased the liver GSH and reduced the liver MDA. Simultaneously, ISP I also acquired anti-oxidative activity in LX-2 cells. Furthermore, we proved the repressor index of ECH1 and demonstrated that ISP I could markedly upregulate the ECH1 pathway in both the BDL model and LX-2 cells. Therefore, all the results certified the anti-oxidative activity of ISP I, which might contribute to its liver-protective and anti-fibrosis effects.

By ABPP assay, we found that ISP I might bind to the target of NUBP2. However, how NUBP2 regulates is unknown. Several previous studies have approved that VNN1 as a pantetheinase, would regulate the generation of cysteamine. Cysteamine can promote the transport of cysteine into cells and is further used to synthesize glutathione. In our study, we found the novelty of the pro-fibrogenic property of VNN1 by overexpression in LX-2 cells. In addition, we further proved ISP I would reduce the binding of VNN1 to NUBP2. Up to now, we suspected that ISP I performed its activity through the NUBP2-VNN1 pathway. By separating the cell membrane proteins, we verified that ISP I increased VNN1 localization to the cell membrane, which majors its action in regulating adapt stress. However, lacking its human crystal structure, the binding sites of ISP I and NUBP2 are still one mystery.

In addition, liver fibrosis severity in steatohepatitis patients was closely correlated with inflammation degree [33]. Injury-induced activation of hepatic inflammation factor is observed in various nonparenchymal cells, including HSCs and Kupffer cells. This study fully discovered the anti-inflammation effect of ISP I. Our results showed that the NF-κB-mediated inflammation pathway was significantly reduced by ISP I treatment. With all the results, we concluded that ISP I partially ameliorates BDL-induced liver damage and fibrosis by suppressing inflammation. Certainly, carrimycin and ISP I may cause antimicrobial resistance or damage to the immune system after long-term taking. If that happens, we recommend

modifying their chemical structure to retain the active group of liver fibrosis and remove other active groups as proposed in the future.

5. Conclusion

Our study demonstrates that ISP I or carrimycin ameliorates liver damage, inflammation, oxidative stress, and fibrosis in animal models and human cells, suggesting that ISP I or carrimycin has therapeutic potential against liver injury and fibrosis. Mechanism study reveals that ISP I decreases the interaction of NUBP2 and VNN1 through binding to the direct target of NUBP2, thus increasing the localization of VNN1 to the cell membrane and producing much more cysteamine. With the upregulation of GSH level and ECH1 expression, as well as the downregulation of MDA and ROS levels, ISP I manifests a precise effect in preventing the development of liver damage and fibrosis by repressing oxidative stress. Therefore, our study provides potential therapeutic agents for patients with liver fibrosis-related diseases, and the clear mechanism supports the wide application in clinics in the future.

CRediT authorship contribution statement

Na Zhang: Writing – original draft, Project administration, Data curation, Conceptualization. **Weixiao Niu:** Software, Project administration, Investigation. **Weiping Niu:** Methodology, Formal analysis, Data curation. **Yiming Li:** Methodology, Formal analysis, Conceptualization. **Simin Guo:** Software, Project administration. **Yang Li:** Supervision, Investigation. **Weiqing He:** Writing – review & editing, Supervision, Investigation, Funding acquisition. **Hongwei He:** Writing – review & editing, Supervision, Project administration, Funding acquisition, Conceptualization.

Declaration of competing interest

The authors declare that there are no conflicts of interest.

Acknowledgments

The study is supported by the Beijing Natural Science Foundation, China (Grant No.: 7222118), the National Natural Science Foundation of China (Grant No.: 82073900), and the CAMS Innovation Fund for Medical Sciences, China (CIFMS, Grant Nos.: 2021–I2M–1–030, and 2021–I2M–1–028).

References

[1] R. Weiskirchen, S. Weiskirchen, F. Tacke, Organ and tissue fibrosis: Molecular signals, cellular mechanisms and translational implications, Mol. Aspects Med. 65 (2019) 2–15.
[2] T. Tsuchida, S.L. Friedman, Mechanisms of hepatic stellate cell activation, Nat. Rev. Gastroenterol. Hepatol. 14 (2017) 397–411.
[3] J.A. Del Campo, P. Gallego, L. Grande, Role of inflammatory response in liver diseases: Therapeutic strategies, World J. Hepatol. 10 (2018) 1–7.
[4] H.J. Forman, H. Zhang, Targeting oxidative stress in disease: Promise and limitations of antioxidant therapy, Nat. Rev. Drug Discov. 20 (2021) 689–709.
[5] Q. Zhang, P. Luo, L. Zheng, et al., 18beta-glycyrrhetinic acid induces ROS-mediated apoptosis to ameliorate hepatic fibrosis by targeting PRDX1/2 in activated HSCs, J. Pharm. Anal. 12 (2022) 570–582.
[6] B. Liu, W. Yi, X. Mao, et al., Enoyl coenzyme A hydratase 1 alleviates nonalcoholic steatohepatitis in mice by suppressing hepatic ferroptosis, Am. J. Physiol. Endocrinol. Metab. 320 (2021) E925–E937.
[7] D. Huang, B. Liu, K. Huang, et al., Enoyl coenzyme A hydratase 1 protects against high-fat-diet-induced hepatic steatosis and insulin resistance, Biochem. Biophys. Res. Commun. 499 (2018) 403–409.
[8] J. Cui, J. Zhou, W. He, et al., Targeting selenoprotein H in the nucleolus suppresses tumors and metastases by Isovalerylspiramycin I, J. Exp. Clin. Cancer Res. 41 (2022), 126.
[9] H. Yan, J. Sun, K. Wang, et al., Repurposing carrimycin as an antiviral agent against human coronaviruses, including the currently pandemic SARS-CoV-2, Acta Pharm. Sin. B 11 (2021) 2850–2858.
[10] Y. Jin, H.X. Zuo, M.Y. Li, et al., Anti-tumor effects of carrimycin and monomeric isovalerylspiramycin I on hepatocellular carcinoma in vitro and in vivo, Front. Pharmacol. 12 (2021), 774231.
[11] N. Zhang, Y. Wu, W. Zhong, et al., Multiple anti-non-alcoholic steatohepatitis (NASH) efficacies of isopropylidenyl anemosapogenin via farnesoid X receptor activation and TFEB-mediated autophagy, Phytomedicine 102 (2022), 154148.
[12] N. Zhang, T. Fan, L. Zhao, et al., Discovery and development of palmatine analogues as anti-NASH agents by activating farnesoid X receptor (FXR), Eur. J. Med. Chem. 245 (2023), 114886.
[13] H. Xiang, F. Guo, X. Tao, et al., Pancreatic ductal deletion of S100A9 alleviates acute pancreatitis by targeting VNN1-mediated ROS release to inhibit NLRP3 activation, Theranostics 11 (2021) 4467–4482.
[14] G. Pitari, F. Malergue, F. Martin, et al., Pantetheinase activity of membrane-bound Vanin-1: Lack of free cysteamine in tissues of Vanin-1 deficient mice, FEBS Lett. 483 (2000) 149–154.
[15] M. Besouw, R. Masereeuw, L. van den Heuvel, et al., Cysteamine: An old drug with new potential, Drug Discov. Today 18 (2013) 785–792.
[16] L. Di Leandro, B. Maras, M.E. Schininà, et al., Cystamine restores GSTA3 levels in Vanin-1 null mice, Free. Radic. Biol. Med. 44 (2008) 1088–1096.
[17] A.D. Read, R.E. Bentley, S.L. Archer, et al., Mitochondrial iron-sulfur clusters: Structure, function, and an emerging role in vascular biology, Redox Biol. 47 (2021), 102164.
[18] C. Wachnowsky, A.L. Hendricks, N.A. Wesley, et al., Understanding the mechanism of[4Fe-4S]cluster assembly on eukaryotic mitochondrial and cytosolic aconitase, Inorg. Chem. 58 (2019) 13686–13695.
[19] M. Fontecave, Iron-sulfur clusters: Ever-expanding roles, Nat. Chem. Biol. 2 (2006) 171–174.
[20] E. Kypri, A. Christodoulou, G. Maimaris, et al., The nucleotide-binding proteins Nubp1 and Nubp2 are negative regulators of ciliogenesis, Cell. Mol. Life Sci. 71 (2014) 517–538.
[21] N. Zhang, S. Zhao, Y. Zhang, et al., A novel biphenyl compound IMB-S7 ameliorates hepatic fibrosis in BDL rats by suppressing Sp1-mediated integrin αv expression, Acta Pharmacol. Sin. 41 (2020) 661–669.
[22] T. Tsuchida, Y.A. Lee, N. Fujiwara, et al., A simple diet- and chemical-induced murine NASH model with rapid progression of steatohepatitis, fibrosis and liver cancer, J. Hepatol. 69 (2018) 385–395.
[23] T. Pradhan-Sundd, K. Kosar, H. Saggi, et al., Wnt/β-catenin signaling plays a protective role in the Mdr2 knockout murine model of cholestatic liver disease, Hepatology 71 (2020) 1732–1749.
[24] H. He, A. Mennone, J.L. Boyer, et al., Combination of retinoic acid and ursodeoxycholic acid attenuates liver injury in bile duct-ligated rats and human hepatic cells, Hepatology 53 (2011) 548–557.
[25] M.J. Ryan, C. Bales, A. Nelson, et al., Bile duct proliferation in Jag1/fringe heterozygous mice identifies candidate modifiers of the Alagille syndrome hepatic phenotype, Hepatology 48 (2008) 1989–1997.
[26] R. Crinelli, C. Zara, L. Galluzzi, et al., Activation of NRF2 and ATF4 signaling by the pro-glutathione molecule I-152, a co-drug of N-acetyl-cysteine and cysteamine, Antioxidants (Basel) 10 (2021), 175.
[27] A. Fraternale, R. Crinelli, A. Casabianca, et al., Molecules altering the intracellular thiol content modulate NF-kB and STAT-1/IRF-1 signalling pathways and IL-12 p40 and IL-27 p28 production in murine macrophages, PLoS One 8 (2013), e57866.
[28] D. Schuppan, M. Ashfaq-Khan, A.T. Yang, et al., Liver fibrosis: Direct antifibrotic agents and targeted therapies, Matrix Biol. 68-69 (2018) 435–451.
[29] S. Zhao, J. Wang, Y. Wang, et al., Establishment and application of a high-throughput drug screening model based on COL1A1 promoter for anti-liver fibrosis, Yao Xue Xue Bao 50 (2015) 169–173.
[30] C.Y. Ma, H.X. Zhou, J.Y. Li, et al., Construction of 4'-isovaleryl spiramycin-I-producing strain by in-frame partial deletion of 3-O-acyltransferase gene in Streptomyces spiramyceticus WSJ-1, the biteSpiramycin producer, Curr. Microbiol. 62 (2011) 16–20.
[31] S. Zhao, N. Li, Y. Zhen, et al., Protective effect of gastrodin on bile duct ligation-induced hepatic fibrosis in rats, Food Chem. Toxicol. 86 (2015) 202–207.
[32] P.L. Jansen, A. Ghallab, N. Vartak, et al., The ascending pathophysiology of cholestatic liver disease, Hepatol. Baltim. Md 65 (2017) 722–738.
[33] P.S. Ribeiro, H. Cortez-Pinto, S. Sola, et al., Hepatocyte apoptosis, expression of death receptors, and activation of NF-kappaB in the liver of nonalcoholic and alcoholic steatohepatitis patients, Am. J. Gastroenterol. 99 (2004) 1708–1717.